ACS APPLIED MATERIALS & INTERFACES

Research Article

www.acsami.org

Charge Separation between Polar {111} Surfaces of CoO Octahedrons and Their Enhanced Visible-Light Photocatalytic Activity

Bin Liu,[†] Lan Ma,[†] Li-Chao Ning,[‡] Cong-Jie Zhang,[‡] Guo-Ping Han,[†] Cui-Jin Pei,[†] Hua Zhao,[†] Sheng-Zhong Liu,[§] and He-Qing Yang*,[†]

[†]Key Laboratory of Macromolecular Science of Shaanxi Province, School of Materials Science and Engineering, Shaanxi Normal University, Xi'an 710119, China

[‡]Key Laboratory of Macromolecular Science of Shaanxi Province, School of Chemistry and Chemical Engineering, Shaanxi Normal University, Xi'an 710119, China

[§]Key Laboratory of Applied Surface and Colloid Chemistry, Ministry of Education, School of Materials Science and Engineering, Shaanxi Normal University, Xi'an 710119, China

Supporting Information

ABSTRACT: Crystal facet engineering of semiconductors has been proven to be an effective strategy to increase photocatalytic performances. However, the mechanism involved in the photocatalysis is not yet known. Herein, we report our success in that photocatalytic performances of the Cl^- ion capped CoO octahedrons with exposed {111} facets were activated by a treatment using $AgNO_3$ and $NH_3{\cdot}H_2O$ solutions. The clean CoO {111} facets were found to be highly reactivity faces. On the basis of the polar structure of the exposed {111} surfaces, a charge separation model between polar {111} surfaces is proposed. There is an internal electric field between polar {111} surfaces due to the spontaneous polarization. The internal electric field provides a driving force for charge separation. The reduction and oxidation reactions selectively take place on the positive and negative polar {111} surfaces. The charge separation model provides a clear insight into charge transfer in the semiconductor nanocrystals with high photocatalytic activities and offer guidance to design more effective photocatalysts, solar cells, photoelectrodes, and other photoelectronic devices.

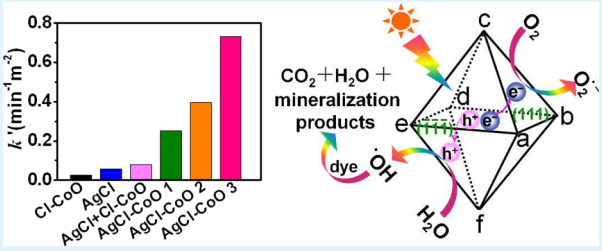

KEYWORDS: *CoO octahedrons, visible-light, photocatalytic activity, charge separation, polar {111} surfaces*

1. INTRODUCTION

Recently, the crystal-facet-controlled fabrication of semiconductor nanomaterials has attracted significant research activities because their photoelectronic and photocatalytic properties can be further enhanced by tailoring the surface atomic structures.[1−14] The {001} facets of anatase TiO_2,[4] BiOCl,[5] $BiVO_4$,[6] β-Bi_2O_3,[7] WO_3,[8] Bi_2WO_6,[9] and CdS,[10] Ag_3PO_4 {110}[11] and InOOH {020} facets,[12] as well as Cu_2O {111}[13] and {522} facets,[14] have been found to exhibit enhanced photocatalytic activities for degradation of toxic organic pollutants, splitting of water and reduction of CO_2. Unfortunately, the underlying principle of the photocatalytic activity is not yet clear.

Cobalt monoxide (CoO) is an important p-type semiconductor with a band gap of 2.2−2.8 eV.[15] It has been used in various fields, such as catalysis,[16] magnetic data storage devices,[17] lithium-ion battery materials,[18,19] and solid-state gas sensors[20] because of its chemical stability and superior magnetic properties. Up to now, CoO nanomaterials with different morphologies have been synthesized, including nanoparticles,[21] -plates,[22] -ribbons,[23] -cubes,[23] -belts,[24] and -spheres;[25] octahedrons;[26] bullet- and pencil-shaped nanorods,[27,28] porous nanowires arrays;[29] and flowerlike structures[30] of CoO. The CoO nanoparticles/graphene nanosheet composites exhibit very high reversible lithium storage capacity and excellent rate capability.[18] In addition, the CoO nanoparticles are found to show superparamagnetism or weak ferromagnetism,[17,21] and can carry out overall water splitting with a solar-to-hydrogen efficiency as high as 5%.[16] However, to the best of our knowledge, the CoO facet-dependent physical and chemical properties have never been reported until now.

Herein, we report on the synthesis of Cl^- ion capped CoO octahedrons with exposed {111} facets (Cl−CoO octahedrons) by heating $CoCl_2$ aqueous solution at 450 °C in a N_2 gas atmosphere. The photocatalytic activity of the Cl−CoO octahedrons for degradation of malachite green (MG) under

Received: December 1, 2014
Accepted: March 3, 2015
Published: March 3, 2015

DOI: 10.1021/am508357x
ACS Appl. Mater. Interfaces 2015, 7, 6109−6117

visible light was enhanced by a treatment using $AgNO_3$ and $NH_3{\cdot}H_2O$ solutions. The enhanced photocatalytic activities are attributed to the clean CoO {111} facets and the heterojunction between AgCl and CoO. The structure and atomic charge of the exposed CoO {111} facets are studied using periodic density functional theory (DFT). It is found that the exposed CoO {111} facets are polar surfaces. A charge separation model between polar {111} surfaces is proposed to explain the enhanced photocatalytic activities.

2. EXPERIMENTAL SECTION

Synthesis of Cl−CoO octahedrons was carried out in a conventional horizontal quartz tube furnace. In a typical experiment, a (111) silicon wafer (p-type with resistivity of 8.1−9.5 Ω·cm) with a dimension of 1.5 × 1.5 cm was cleaned with deionized water and absolute ethanol in an ultrasound bath for 15 min, respectively. Two or three drops of 0.50 mol/L $CoCl_2$ aqueous solutions were added on the silicon wafer in a quartz boat. The boat was positioned at the center of the furnace. Prior to heating, high-purity N_2 (99.999%) was introduced into the quartz tube at a constant flowing rate of 2.5 L/h to purge the tube. After 15 min, the furnace was heated at a rate of 20 °C min^{-1} to 450 °C and kept for 1 h under a constant N_2 flow of 1.5 L/h. After the system cooled to room temperature under N_2 flow of 1.5 L/h black products were observed on the Si wafer.

Preparation of CoO octahedrons with loaded AgCl particles (AgCl−CoO octahedrons): In a typical process, 10 mg of the as-synthesized Cl−CoO octahedrons and 25.0, 50.0, 75.0, or 150.0 mL of 0.01 mol/L of $AgNO_3$ solution were put into a 100 or 400 mL beaker. The mixture was stirred for 30 min then allowed to stand for 2 h in the dark. The products were collected by centrifugation and then dried naturally in the dark.

Preparation of AgCl particles: In a typical process, 2.5 mL of 1.0 mol/L $AgNO_3$ solution and 2.5 mL of 1.0 mol/L NaCl solution were added into a 50 mL beaker, the mixed solution then was stirred for 15 min to form a white precipitate. The white precipitate was collected by centrifugation and dried in the dark at 60 °C. All reagents used were of analytical grade and were directly used without further purification.

The as-prepared products were characterized and analyzed using powder X-ray diffraction (XRD), scanning electron microscopy (SEM), transmission electron microscopy (TEM) and X-ray photoelectron spectra (XPS). The XRD analysis was performed using a DX-2700 X-ray diffractometer equipped with Cu Kα_1 radiation (λ = 1.541 Å) at 40 kV and 30 mA. Each specimen was scanned at a step size of 0.02° and a scanning speed of 4°/min with diffraction angles between 20 and 70°. SEM images were obtained using an FEI Quanta 200 scanning electron microscope at an accelerating voltage of 20 kV. Energy-dispersive X-ray spectroscopy (EDX) facilities attached to the SEM were employed to analyze chemical composition. TEM and electron diffraction images were obtained using a JEOL JEM-3010 TEM at an accelerating voltage of 300 kV. The samples for TEM were prepared by dispersing Cl−CoO and AgCl−CoO octahedron powders on a carbon-coated copper grid. XPS measurements were performed by using a Kratos Axis ultra X-ray photoelectron spectrometer with an excitation source of Al Kα = 1486.7 eV. The binding energies obtained in the XPS analysis were corrected for specimen charging through referencing the C 1s to 284.6 eV. The Brunauer−Emmett−Teller (BET) specific surface area measurement was performed by N_2 gas adsorption using an America Micromeritics ASAP 2020 surface analytical instrument. The diffuse reflectance spectrum of the products was obtained on a Perkin−Elmer Lambd 950 spectrophotometer.

The crystal structure of cubic CoO was calculated using the DMOL3 code[31] and the generalized gradient approximation (GGA) with Perdew−Burke−Ernzerhof (PBE) functional is employed as the exchange-correlation functional.[32] The atomic charges are computed using Hirshfeld[33] population analyses. The surface energy was computed using the formula[34]

$$E_{surface} = \frac{E_{slab} - nE_{bulk}}{2A}$$

where E_{slab} is the total energy of the slab, E_{bulk} is the total energy of the bulk per unit cell, n is the number of bulk unit cells contained in the slab, and A is the surface area of each side of the slab, the 1/2 factor is used to obtain the average value of the surface energies of the top and bottom of the slab.

Evaluation of photocatalytic activity: MG with a molecular weight of 927 is selected as model organic compounds to examine the photocatalytic activity of the AgCl−CoO octahedron structures, 10.0 mg of the as-prepared photocatalyst (sample 1−4) was added to 10.0 mL 1.0 × 10^{-5} mol/L MG solution to get a suspension. The suspension was magnetically stirred for 10 min in the dark to establish an adsorption/desorption equilibrium between the dye and the photocatalyst. Then, the mixed solution was irradiated by a Xe lamp (500 W) equipped with an optical filter ($\lambda \geq$ 420 nm) to cut off the ultraviolet light (XPA-7 photochemical reactor, Xujiang Electromechanical Plant, Nanjing, China). After each regular irradiation time interval, 5 mL of sample was withdrawn from the test tube for analysis. The sample is first purified by centrifugation to remove any particulates, and then the absorption spectra were measured using a U-2910 ultraviolet−visible spectrophotometer (Hitachi High-Technologies Corp., Tokyo, Japan) using deionized water as a reference. For comparison, the photocatalytic activities of Cl−CoO octahedrons, AgCl particles and the mixture of Cl−CoO octahedrons and AgCl particles were also tested under the same conditions and with the equal mass of catalyst as that employed for AgCl−CoO octahedrons.

3. RESULTS AND DISCUSSION

3.1. Morphology and Crystal Structure of Cl−CoO Octahedrons. The morphology and crystal structure of the as-prepared samples were investigated by SEM and XRD, and the results are shown in Figure 1. Figure 1a,b shows typical SEM images of the samples grown at 450 °C for 1 h; the images show that the samples consist of a large quantity of regular octahedron structures. The exposed facets are close to an equilateral triangle, and the edge lengths are in the range of 0.63−1.8 μm. The EDX spectrum is shown in Figure 1c, and the element map are shown in Figure S1 (Supporting Information). The results reveal that the samples contain Co,

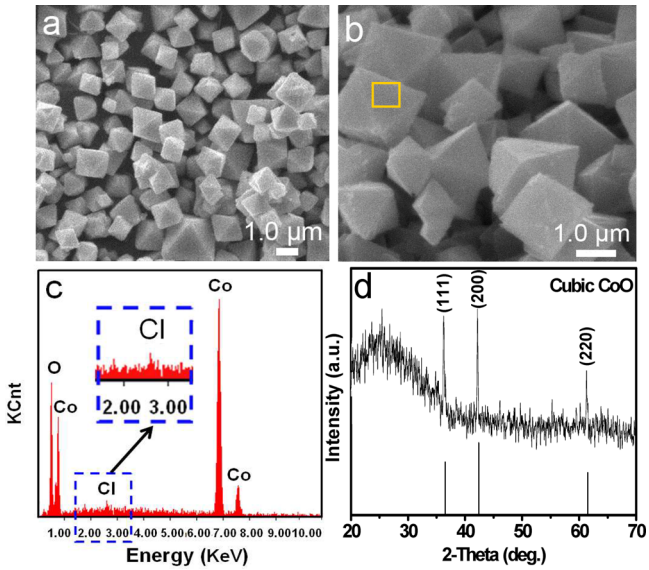

Figure 1. (a and b) SEM images of Cl−CoO octahedrons obtained by heating $CoCl_2$ solution at 450 °C for 1 h. (c) EDX spectrum from the box in panel b. (d) XRD pattern of the as-obtained Cl−CoO octahedrons. The stick pattern in d is the standard XRD pattern of cubic CoO powders with Cu Kα radiation (JPCDS card no. 65-2902).

DOI: 10.1021/am508357x
ACS Appl. Mater. Interfaces 2015, 7, 6109−6117

O, and Cl elements, and elemental Cl may exist at the surface of CoO octahedrons. The corresponding XRD pattern is shown in Figure 1d. According to the Joint Committee on Powder Diffraction Standards (JCPDS) card No. 65-2902, the peaks at 2θ = 36.5, 42.3, and 61.5° are assigned to (111), (200), and (220) diffraction lines of the cubic CoO, respectively. In addition, the present CoO octahedrons show markedly higher intensity ratios of (111) to other diffraction peaks in comparison with those from the standard pattern of the cubic CoO powder samples, demonstrating strong (111) preferred orientation. The texture coefficient (TC) of (111) plane is defined as[12]

$$\mathrm{TC}(111) = \frac{I(111)}{I_0(111)}\left\{\frac{1}{n}\sum\frac{I(hkl)}{I_0(hkl)}\right\}^{-1}$$

where $I(hkl)$ is the measured intensity of the (hkl) reflection, $I_0(hkl)$ is the powder diffraction intensity of the cubic CoO according to the JPCDS card no. 65-2902, and n is the number of diffraction peaks used in the calculation. For materials with random crystallographic orientations (e.g., powders), the texture coefficient of any (hkl) reflection should be 1. The texture coefficient of the (111) plane of the CoO octahedron is 1.52, an obvious strong indication of (111) preferred orientation.

The XPS spectra of the as-prepared Cl−CoO octahedrons are shown in Figure 2, including (a) the survey spectrum, (b)

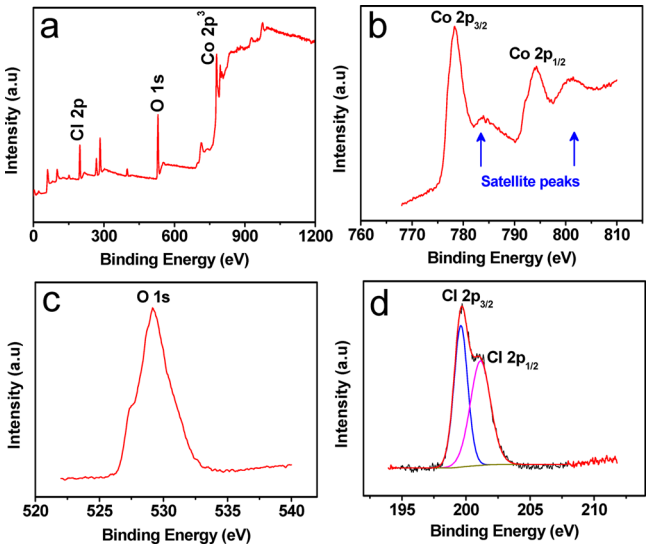

Figure 2. XPS spectra of Cl−CoO octahedrons obtained by heating $CoCl_2$ aqueous solution at 450 °C for 1 h in N_2 gas atmosphere.

Co $2p_{3/2}$ and $2p_{1/2}$, (c) O 1s, and (d) Cl $2p_{3/2}$ and $2p_{1/2}$. The binding energy of Co $2p_{3/2}$ and $2p_{1/2}$, is identified at 778.4 and 794.0 eV, respectively. Nevertheless, satellite structures apart from the main peaks are evident of Co(II) existence.[16] The peak at 530.8 eV corresponds to O 1s. The peaks at 199.4 and 200.8 eV can be assigned to Cl $2p_{3/2}$ and $2p_{1/2}$, respectively,[35] which might come from the surface Cl^- ions of CoO octahedrons. The XPS spectra and EDX analysis suggest that the formation of the CoO octahedrons may originate from the selective adsorption of Cl^- ions.

Figure 3a shows a typical TEM image of an [100] orientated CoO octahedron when the electron beam is aligned to ⟨100⟩. The edge length is about 1.7 μm in good agreement with the

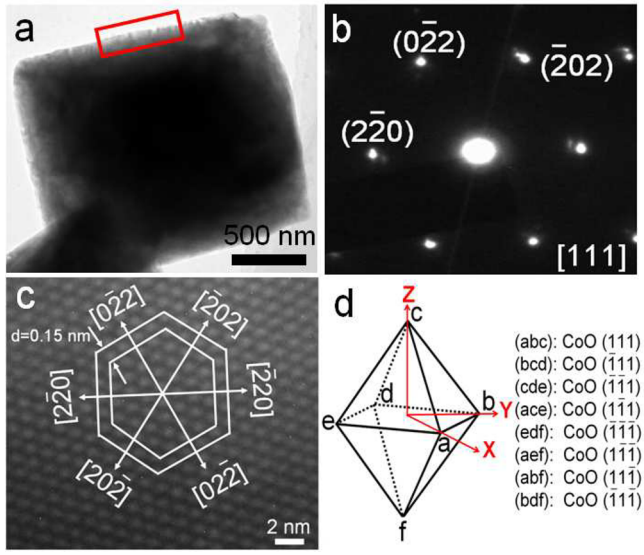

Figure 3. (a) TEM image of an [100] orientated CoO octahedron when the electron beams is aligned to ⟨100⟩. (b) SAED pattern and (c) HRTEM image from the box in panel a. (d) The schematic illustration of crystal orientation of the CoO octahedron.

SEM observation. Figure 3b shows the selected area electron diffraction (SAED) pattern taken from the box in panel (a). It is indexed as the [111] zone axis of single-crystalline CoO with a cubic structure. The high-resolution TEM (HRTEM) image shown in Figure 3c gives a lattice spacing of 0.15 nm, corresponding to the d spacing of (2$\bar{2}$0) crystal planes of cubic phase. The results indicate that the CoO octahedron is enclosed by (111), ($\bar{1}$11), ($\bar{1}\,\bar{1}$1), (1$\bar{1}$1), ($\bar{1}\,\bar{1}\,\bar{1}$), (1$\bar{1}\,\bar{1}$), (11$\bar{1}$) and ($\bar{1}\,\bar{1}\,\bar{1}$) faces, and the schematic illustration of the crystal orientation is shown in Figure 3d. In addition, there is a large quantity of Cl^- ions on the surface of the octahedrons.

3.2. Formation Mechanism of Cl−CoO Octahedron Structures. CoO crystal has a NaCl-type structure, the conceptually simple structure is commonly known as the rock salt structure, the model for which is shown in Figure 4a. The structure of CoO (111) facet obtained from periodic DFT calculations is shown in Figure 4b. It is clearly observed that the (111) surface termination consists of a layer of unsaturated Co sites, and each Co atom on the (111) plane is three-coordinated. The ($\bar{1}$11), ($\bar{1}\,\bar{1}$1), and (1$\bar{1}$1) surface structures are the same as the (111) surface. In the present system, Cl^- ions may serve as a ligand to Co^{2+}, and adsorb selectively on unsaturated Co sites on the CoO (111), ($\bar{1}$11), ($\bar{1}\,\bar{1}$1), and (1$\bar{1}$1) surface. The most likely structure is described in Figure 4c. The presence of Cl^- ions impedes the growth of the {111} surfaces. When the ratio of the growth rate in the ⟨100⟩ to that of the ⟨111⟩ equals to ~1.73, perfect octahedrons are obtained.[36]

3.3. Morphology and Crystal Structure of AgCl−CoO Octahedrons. The products prepared by the reaction of the Cl−CoO octahedrons with various volumes of $AgNO_3$ solutions were summarized in Table 1. The SEM images, EDX spectrum, and XRD pattern from sample 3 are shown in Figure 5. The SEM images (Figure 5a,b) reveal that sample 3 is composed of a large quantity of octahedrons with edge lengths of 1.3−1.8 μm. There are some nanoparticles 40−80 nm in size on the surface of the CoO octahedrons. The EDX spectrum from box in panel b is shown in Figure 5c, indicating that the

DOI: 10.1021/am508357x
ACS Appl. Mater. Interfaces 2015, 7, 6109−6117

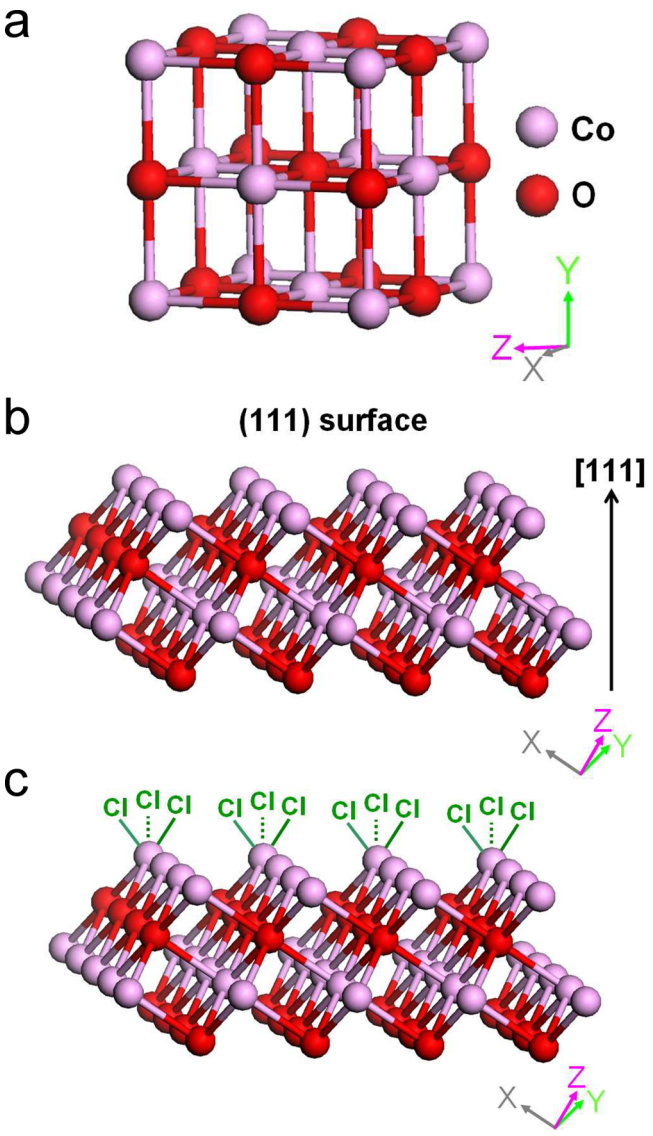

Figure 4. (a) Cubic CoO crystal structure. (b) The atomic structures of (111) surfaces obtained from periodic DFT calculations. (c) The structure of the Cl^- ions attached to unsaturated Co^{2+} sites on the (111) prismatic faces.

Table 1. AgCl−CoO Octahedrons Obtained by the Reaction of the Cl−CoO Octahedrons with Various Volumes of $AgNO_3$ Solutions

	sample number			
	1	2	3	4
weight of Cl−CoO octahedron (mg)	10	10	10	10
volume of $AgNO_3$ solution (mL)[a]	25	50	75	150

[a]Concentration of $AgNO_3$ solution is 1.0×10^{-2} mol/L.

octahedron consist of Co, O, Ag, and Cl elements. The corresponding XRD pattern is presented in Figure 5d, indicating that the as-obtained products (sample 3) are cubic structured AgCl-cubic phase CoO composite. The TEM images for sample 3 are shown in Figure 6a,b. It was found that the sample is very sensitive to electron irradiation. Under electron beam irradiation, the surface with the AgCl nanoparticles is so unstable that it can be removed quickly from surface of the CoO octahedron. The SAED pattern and HRTEM image from

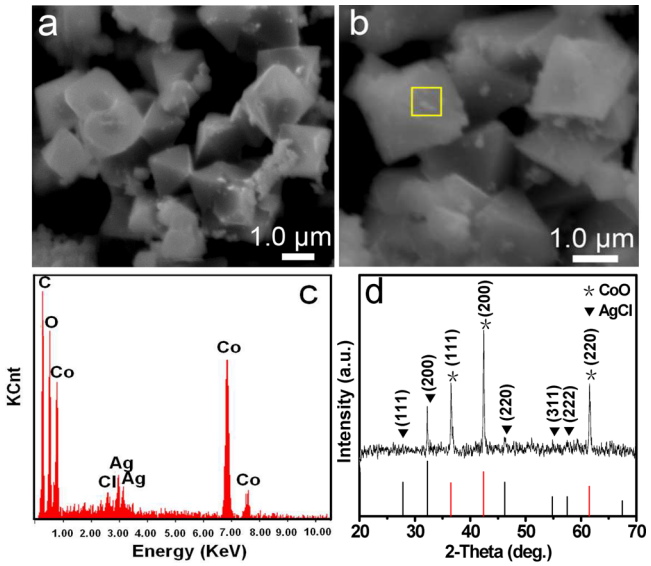

Figure 5. (a and b) SEM images of sample 3. (c) EDX spectrum from the box in panel b. (d) XRD pattern of sample 3. The stick patterns in d are the standard XRD pattern of cubic CoO and AgCl powders with Cu Kα radiation (JPCDS card nos. 65-2902 and 31-1238).

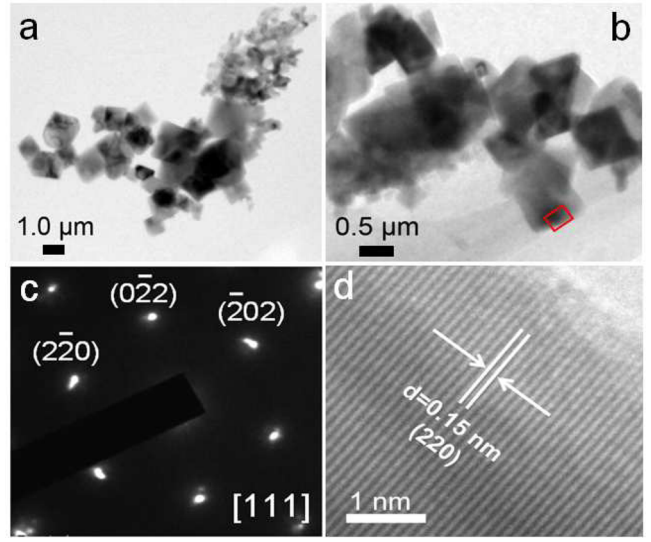

Figure 6. (a and b) TEM images of the sample 3. (c) SAED pattern and (d) HRTEM image from the box in panel b.

the box in panel b are shown in Figure 6c,d and indicates that, after the removal of AgCl, the CoO octahedron is enclosed by {111} facets. It appeared that the AgCl particles capped on the surface of CoO octahedrons.

SEM image and XRD pattern of the as-prepared AgCl particles are shown in Figure S2, Supporting Information. It is clear that the as-obtained products consist of a large quantity of cubic AgCl particles with 295−648 nm in size.

3.4. Photocatalytic Activity. We selected the characteristic absorption of MG at 616 nm monitoring the adsorption and photocatalytic degradation over the as-prepared Cl−CoO octahedrons, AgCl−CoO octahedrons (samples 1−4) and AgCl particles. Before evaluating of the photocatalytic activity, we carefully studied the adsorption capacity of sample 3, Cl−CoO octahedrons, and AgCl particles for MG; the results are shown in Figure S3 (Supporting Information). The C_0 and C

DOI: 10.1021/am508357x
ACS Appl. Mater. Interfaces 2015, 7, 6109−6117

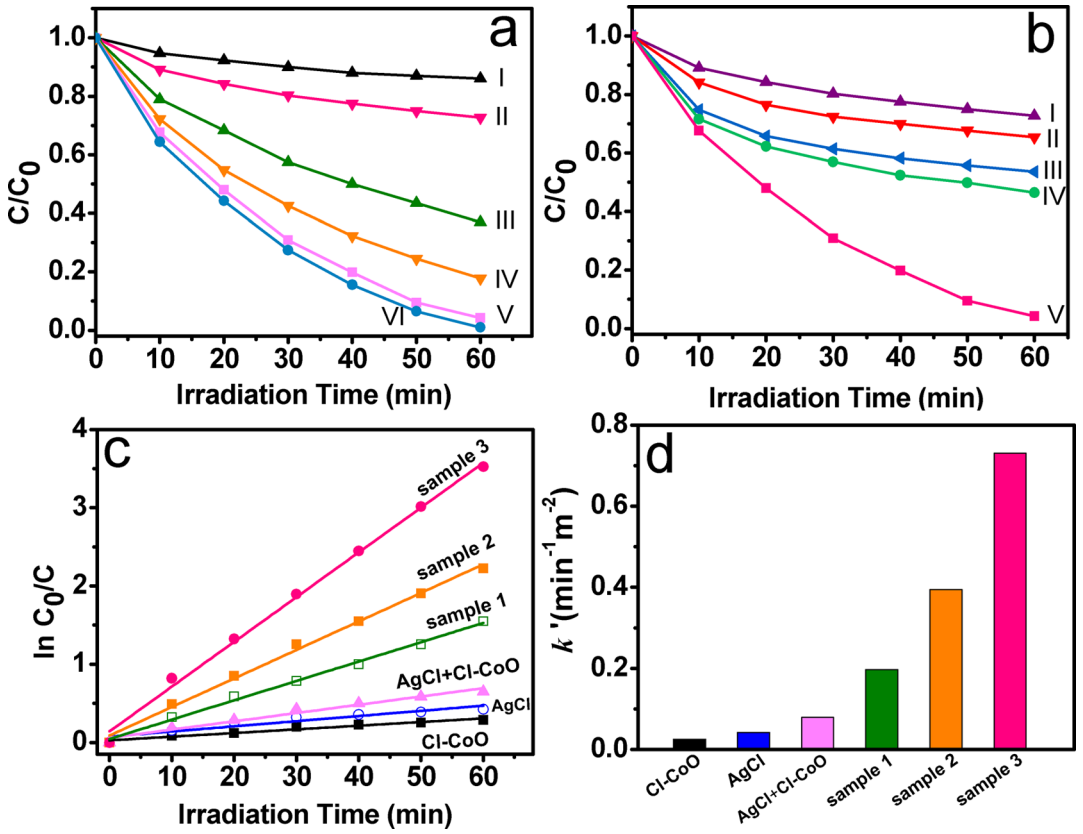

Figure 7. (a) Photodegradation of the MG (I) without catalyst and (II) over Cl−CoO octahedron and samples (III) 1, (IV) 2, (V) 3, (VI) and 4 under Xe lamp irradiation ($\lambda \geq 420$ nm). (b) Photodegradation of the MG over 10.0 mg of (I) Cl−CoO octahedrons, (II) 10 mg of AgCl particles, (III) the mixture of 9.5 mg of Cl−CoO octahedrons and 0.5 mg of AgCl particles, (IV) the mixture of 9.0 mg of Cl−CoO octahedrons and 1.0 mg of AgCl particles, and (V) 10 mg of sample 3 under Xe lamp irradiation ($\lambda \geq 420$ nm). (c) The fitting of ln (C_0/C) plot vs time over Cl−CoO octahedrons, AgCl particles, mixture of AgCl particles and Cl−CoO octahedrons as well as samples 1−3. (d) Normalized apparent rate constant of the degradation per unit surface area (k') over Cl−CoO octahedrons, AgCl particles, the mixture of AgCl particles and Cl−CoO octahedrons as well as samples 1−3.

Table 2. BET Specific Surface Area, k, and k' of Cl−CoO Octahedrons, AgCl Particles, the Mixture of AgCl Particles and Cl−CoO Octahedrons, as well as Samples 1−3

	sample 1	sample 2	sample 3	AgCl + Cl−CoO[a]	AgCl	Cl−CoO
specific surface area (m^{-2} g^{-1})	9.77	9.24	7.83	13.40	11.61	18.22
k (min^{-1})	0.0247 ± 0.0007	0.0365 ± 0.0011	0.0572 ± 0.0017	0.0106 ± 0.0008	0.0066 ± 0.0009	0.0046 ± 0.0004
k' ($min^{-1}m^{-2}$)[b]	0.2528	0.3950	0.7305	0.0794	0.0568	0.0252

[a]AgCl+Cl−CoO: The mixtures of AgCl particles and Cl−CoO octahedrons. [b]k': Normalized apparent rate constant of the degradation per unit surface.

represent the concentration of MG at initial and any time, respectively. For sample 3, Cl−CoO, and AgCl, after 10 min, the value of C/C_0 was 0.94, 0.95, and 0.95, respectively, and it hardly changes, even over an extended period of time, indicating that an adsorption/desorption equilibrium between the dye and the photocatalysts is achieved within 10 min. Therefore, the suspension containing the dye and the catalysts was stirred for 10 min in the dark before the visible light irradiation ($\lambda \geq 420$ nm) to establish an adsorption/desorption equilibrium between the dye and the photocatalyst.

Figure 7a shows the decomposition of MG in solution without catalyst and over Cl−CoO octahedrons, as well as samples 1−4 under visible light irradiation as a function of time. It shows that as the irradiation time increases, the decomposition of MG progress hardly progress without catalyst (curve I), and the decomposition of MG progress slowly over Cl−CoO octahedrons (curve II). However, the decomposition of MG progresses fleetly in the presence of AgCl−CoO octahedrons (samples 1−4, curves III−VI). The decomposition rates for samples 3 and 4 are almost the same, are remarkably faster than those for samples 1 and 2. Moreover, we investigated photocatalytic activities of the AgCl particles and the mixtures of AgCl particles and Cl−CoO octahedrons, compared with sample 3. The results are shown in Figure 7b. Apparently, the decomposition rate of MG over sample 3 is faster than those for the mixtures of AgCl particles and the Cl−CoO octahedrons, AgCl particles and Cl−CoO octahedrons. The fittings of ln (C_0/C) plot vs time over Cl−CoO octahedrons, AgCl particles, the mixture of AgCl particles and Cl−CoO octahedrons as well as samples 1−3 are shown in Figure 7c. The photodegradation of MG catalyzed by the six kinds of catalysts can be explained using pseudo first-order reaction, that is, ln (C_0/C) = kt, where k is the apparent rate constant of the degradation. In our experiment, the k value is

DOI: 10.1021/am508357x
ACS Appl. Mater. Interfaces 2015, 7, 6109−6117

found to be 0.0046 ± 0.0004 for Cl−CoO octahedrons, 0.0066 ± 0.0009 for AgCl particles, 0.016 ± 0.0008 for the mixture of AgCl particles, and Cl−CoO octahedrons, 0.0247 ± 0.0007 for sample 1, 0.0365 ± 0.0011 for sample 2, and 0.0572 ± 0.0017 min^{-1} for sample 3 (Table 2).

It is generally accepted that the catalytic process is mainly related to the absorption and desorption of molecules on the catalyst surface. The BET surface areas of Cl−CoO octahedrons, AgCl particles, the mixture of AgCl particles and Cl−CoO octahedrons, and samples 1−3, were measured to be 18.22, 11.61, 13.40, 9.77, 9.24, and 7.83 $m^2 g^{-1}$, respectively (Table 2). The apparent rate constant the degradation per unit surface area for the six kinds of catalysts, as for the basis for the comparison, is examined in this work. The normalized rate constant values k' of samples 1−3 are higher than that for the Cl−CoO octahedrons, AgCl particles, and the mixture of AgCl particles and Cl−CoO octahedrons, and the k' values for sample 3 is the highest, as seen in Figure 7d and Table 2. The results show that the AgCl−CoO octahedrons exhibit higher photocatalytic activity than Cl−CoO octahedrons, AgCl particles, and the mixture of AgCl particles and Cl−CoO octahedrons, and its photocatalytic activity is enhanced with increasing volume of the $AgNO_3$ solution. When the $AgNO_3$ solution volume is increased to 150 mL, the photocatalytic activity reaches a saturated value. Furthermore, the photocatalytic performance of the Cl−CoO octahedrons treated by $NH_3{\cdot}H_2O$ solution was investigated, and the results are shown in Figure 8a. It was found that the photocatalytic activity is increased by the $NH_3{\cdot}H_2O$ treatment. CoO octahedrons with clean {111} facets were prepared by the reaction of AgCl−CoO octahedrons (sample 3) with 3.0 mol/L $NH_3{\cdot}H_2O$ solution. The as-obtained products were characterized using SEM, EDX and XRD, and the results are shown in Figure S4 (Supporting Information). The SEM observations reveal that the as-obtained products consist of a large quantity of regular CoO octahedron structures with the edge lengths of 1.00−1.78 μm. The exposed {111} facets of the CoO octahedrons are clean surfaces free of Cl^- ions or AgCl particles. We investigated photocatalytic activities of the CoO octahedrons with clean {111} facets compared with sample 3 and Cl−CoO octahedrons, and the results are shown in Figure 8b. It can be seen that the CoO octahedrons with clean {111} facets show higher photocatalytic activity than that of Cl−CoO octahedrons but lower than that of sample 3. We therefore conclude that the enhanced photocatalytic activities of the AgCl−CoO octahedrons may result from the removal of the surface Cl^- ions and loading of AgCl.

In addition, the diffuse reflectance spectra of the Cl−CoO octahedrons, the mixture of AgCl particles and Cl−CoO octahedrons, as well as samples 1, 2, and 3, were measured, as shown in Figure S5a (Supporting Information). As a crystalline semiconductor, the optical absorption near the band edge follows the formula[37]

$$\alpha h\nu = A(h\nu - E_g)^{n/2}$$

where α, ν, E_g and A are the absorption coefficient, light frequency, band gap energy, and a constant, respectively. Among them, n depends on the characteristics of the transition in a semiconductor, that is, direct transition (n = 1) or indirect transition (n = 4). For CoO, the value of n is 1 for direct transition.[16] The band gap energy (E_g value) can be thus estimated from a plot of $(\alpha h\nu)^2$ versus photon energy ($h\nu$; Figure S5b, Supporting Information), and the result of the Cl−CoO octahedrons, the mixture of AgCl particles and Cl−CoO octahedrons, and samples 1−3 was found to be 1.10, 1.13, 1.11, 1.14, and 1.15 eV, respectively. The diffuse reflectance spectra suggest that the superior photocatalytic activities of the AgCl−CoO octahedrons may result from the effective separation of photogenerated charges instead of good light absorption.

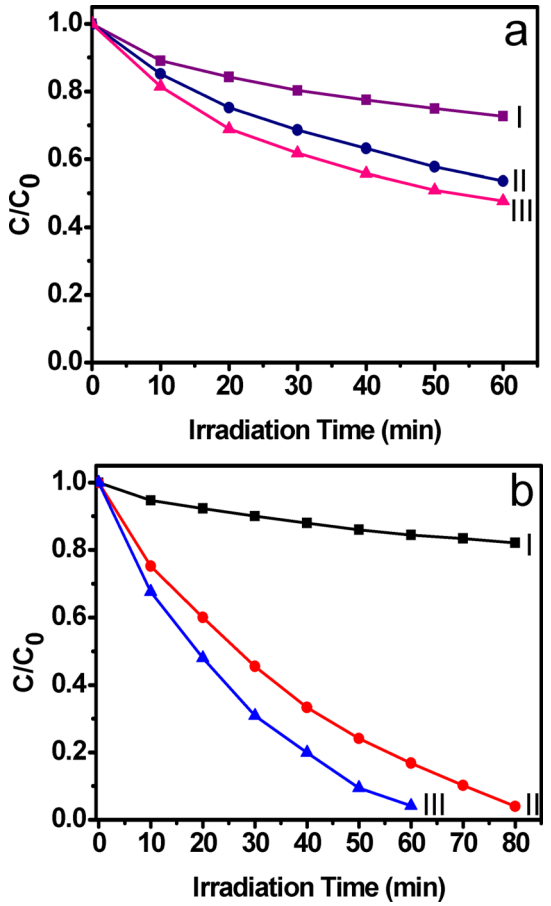

Figure 8. (a) Photodegradation of the MG over (I) Cl−CoO octahedrons, over (II) and (III) Cl−CoO octahedrons treated by 30.0 mL of 1.0 and 2.0 mol/L $NH_3{\cdot}H_2O$ solutions under Xe lamp irradiation ($\lambda \geq 420$ nm). (b) Photodegradation of the MG over (I) Cl−CoO, (II) CoO octahedrons with clean {111} facets, and (III) sample 3 under Xe lamp irradiation ($\lambda \geq 420$ nm).

3.5. Charge Separation between Polar CoO {111} Surfaces and Photocatalysis Mechanism. Surface energy of the CoO {111}, {200}, and {220} facets was calculated using DFT. It is found that CoO {111} facet has much higher surface energy, 2.40, compared to 1.08 and 1.64 J/m^2 for (200) and (220) facets, respectively, which suggests that {111} facets may show higher reactivity than {200} and {220} facets. On the basis of the above experimental results and theory analysis, we conclude that the clean CoO {111} facets are highly reactivity facets. Moreover, the heterojunction between AgCl and CoO contributes to increase in the photocatalytic activity. For the CoO octahedron structure, the exposed {111} facets include four pairs of polar surfaces, they are positive Co-terminated CoO (111), $(\bar{1}11)$, $(1\bar{1}1)$, and $(11\bar{1})$ surfaces and negative O-terminated CoO $(\bar{1}\bar{1}\bar{1})$, $(\bar{1}1\bar{1})$, $(1\bar{1}\bar{1})$, and $(\bar{1}\bar{1}1)$ surfaces, respectively, as shown in Figures 3d and 4b. Atomic charge distribution of the CoO (111) and $(\bar{1}\bar{1}\bar{1})$ surfaces obtained from periodic DFT calculations is shown in Figure 9a. Each

DOI: 10.1021/am508357x
ACS Appl. Mater. Interfaces 2015, 7, 6109−6117

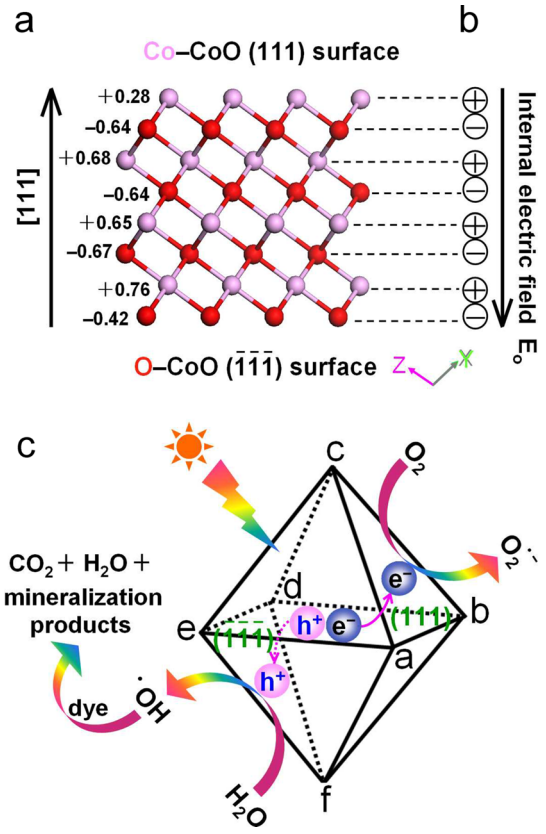

Figure 9. (a) Atomic charge distribution of CoO (111) and ($\bar{1}\bar{1}\bar{1}$) facets obtained by DFT calculations and (b) the equivalent polar chain. (c and d) Schematic illustration of charge separation between polar {111} surfaces and photocatalytic reactions.

layer contains all positive Co^{2+} ions or all negative O^{2-} ions in [111] direction, and the polar chain is shown in Figure 9b. Co atomic charge on the Co–CoO (111) surface is +0.28 and O on the O–CoO ($\bar{1}\,\bar{1}\,\bar{1}$) surface is −0.42. An internal electric field thus is established between each pair of polar {111} surfaces by the spontaneous polarization. A charge separation model between polar {111} surfaces is thus proposed to explain the enhanced photocatalytic activities.

When the CoO octahedrons with exposed {111} polar facets were employed as a photocatalyst, the visible light irradiation induces a transition of electrons from the valence-band to the conduction-band, leaving an equal number of vacant sites (holes), and thus electron–hole pairs were formed in CoO octahedron (Figure 9c, eq 1).[38] The photogenerated electrons and holes migrate to positive polar Co–CoO (111), ($\bar{1}$11), ($\bar{1}\,\bar{1}$1), and (1$\bar{1}$1) and negative polar O–CoO ($\bar{1}\,\bar{1}\,\bar{1}$), (1$\bar{1}\,\bar{1}$), (11$\bar{1}$), and (1$\bar{1}\bar{1}$) surfaces, respectively, under the internal electric field (Figure 9c). The electrons on the positive polar Co–CoO (111), ($\bar{1}$11), ($\bar{1}\,\bar{1}$1), and (1$\bar{1}$1) surfaces are usually scavenged by O_2 to yield superoxide radical anions $O_2^{\bullet-}$ (eq 2).[39] The holes on the negative O–CoO ($\bar{1}\,\bar{1}\,\bar{1}$), (1$\bar{1}\,\bar{1}$), (11$\bar{1}$), and (1$\bar{1}\bar{1}$) surfaces can react with surface adsorbed H_2O to produce $^{\bullet}OH$ radicals (eq 3), the dye molecules then are oxidized into CO_2, H_2O and mineralization products by $^{\bullet}OH$ radicals (eq 4).[39,40]

$$CoO + h\nu \rightarrow CoO(e_{CB}^{-} + h_{VB}^{+}) \quad (1)$$

$$e_{CB}^{-} + O_2 \rightarrow O_2^{\bullet-} \quad (2)$$

$$h_{VB}^{+} + H_2O \rightarrow H^{+} + {}^{\bullet}OH \quad (3)$$

$$^{\bullet}OH + \text{dye} \rightarrow CO_2 + H_2O + \text{mineralization products} \quad (4)$$

The good charge separation can effectively reduce the probability of recombination of photogenerated electrons and holes, and thus, the CoO octahedrons with exposed {111} facets show excellent photocatalytic performance. However, when Cl^- ions are adsorbed selectively on unsaturated Co sites on (111), ($\bar{1}$11), ($\bar{1}\,\bar{1}$1), and (1$\bar{1}$1) surfaces of CoO octahedrons, the surface Cl atom is negatively charged with −0.17, as shown in Figure S6a (Supporting Information). The internal electric field decreases between the {111} polar surfaces, and thus, the Cl–CoO octahedrons show poor photocatalytic activity. When the Cl–CoO octahedrons reacted with $NH_3{\cdot}H_2O$ solution, the surface Cl^- ions were replaced by NH_3 molecules due to the strong coordinating effect of NH_3. The internal electric field are increased because the negative charge of NH_3 molecule is less than that of Cl^- ion, and thus, photocatalytic performance of the Cl–CoO octahedrons is enhanced by the $NH_3{\cdot}H_2O$ solution treatment.

When the surface Cl^- ions reacted with Ag^+ ions to form AgCl, Co atoms on the Co–CoO (111) planes show positive charge, the strong internal electric field between the {111} polar surfaces are renewed. At the same time a heterojunction was formed between AgCl and positive polar Co–CoO facet. The heterojunction improves further the separation of photogenerated electrons and holes, like the *p*-type NiO/*n*-type ZnO,[41] α-Fe_2O_3/NiO,[42] and MoS_2/CdS[43] heterojunctions. The photogenerated electrons transfer further from the Co–CoO facets of CoO to the surface of AgCl particles. The reduction and oxidation reactions selectively take place on the surfaces of AgCl particles and negative polar O–CoO surfaces (Figure S6b, Supporting Information), and thus, AgCl–CoO octahedrons show the enhanced photocatalytic activities.

Moreover, we carried out the MG bleaching experiment repeatedly four times by using sample 3 as a catalyst. As shown in Figure 10, their photocatalytic activity was lightly lowered after four cycles, which indicated that the as-prepared AgCl–CoO octahedrons exhibit remarkable photocatalytic stability. After four cycles sample 3 was characterized with SEM, XRD and XPS, and the results are shown in Figure S7 (Supporting Information). The SEM and XRD observations indicate that

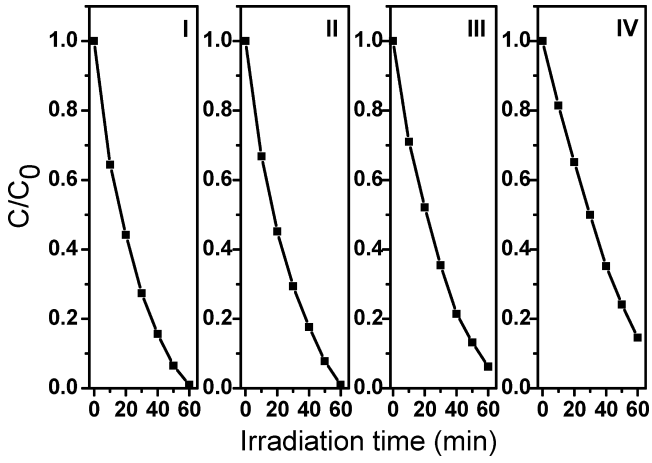

Figure 10. Cyclic photodegradation of the MG solution with sample 3 under Xe lamp irradiation ($\lambda \geq 420$ nm).

DOI: 10.1021/am508357x
ACS Appl. Mater. Interfaces 2015, 7, 6109–6117

after the photocatalytic test the products still consist of octahedron structures. In addition to CoO and AgCl, Ag element was formed. A small quantity of AgCl particles was found to remove from surface of the CoO octahedron by comparing with SEM images of sample 3 in Figure 5a,b. In the Co 2p XPS spectrum, two relatively stronger satellite features with respect to $2p_{3/2}$ and $2p_{1/2}$ further confirm the CoO chemical nature. The removal of AgCl may result in the decrease in the photocatalytic activity.

4. CONCLUSIONS

In summary, we successfully fabricated single crystalline CoO octahedrons capped by Cl^- ions by heating aqueous $CoCl_2$ solution. This simple approach to fabricate CoO octahedrons can be easily scaled up and potentially extended to the synthesis of other oxides. Photocatalytic performance of the CoO octahedrons with exposed {111} facets was activated by a treatment using $AgNO_3$ and $NH_3{\cdot}H_2O$ solutions. The excellent photocatalytic activities are attributed to the clean CoO {111} facets and the heterojunction between AgCl and CoO. On the basis of the polar structure of the CoO {111} surfaces, a charge separation model between polar {111} surfaces is proposed. Our results demonstrate that it is feasible to increase photocatalytic property of cubic structured CoO by selectively exposing the polar {111} facets. In addition, we may design and fabricate more effective photocatalysts and new types of photoelectrodes, solar cells, or photoelectric devices by the surface-engineering strategy.

■ ASSOCIATED CONTENT

Supporting Information

Elemental mapping of the Cl−CoO octahedrons, SEM image and XRD pattern of AgCl particles, adsorption kinetics of MG on various samples, preparation and characterization of CoO octahedrons with clean {111} facets, the diffuse reflectance spectra and the plot of $(\alpha h\nu)^2$ versus photon energy $(h\nu)$ of various samples, atomic charge distribution of Cl−CoO, the schematic illustration of photocatalytic reactions on the CoO octahedrons with loaded AgCl particles and characterization of sample 3 after four cycles. This material is available free of charge via the Internet at http://pubs.acs.org.

■ AUTHOR INFORMATION

Corresponding Author

*Fax: 0086-29-81530702. E-mail: hqyang@snnu.edu.cn.

Notes

The authors declare no competing financial interest.

■ ACKNOWLEDGMENTS

This work was supported by the National Natural Science Foundation of China (Grant No. 21073116), the Natural Science Foundation of Shaanxi Province (Grant No. 2013JZ002), and the Fundamental Research Funds for the Central Universities (Grant Nos. GK201101004 and GK201402019).

■ REFERENCES

(1) Jiang, Z. Y.; Kuang, Q.; Xie, Z. X.; Zheng, L. X. Syntheses and Properties of Micro/Nanostructured Crystallites with High-Energy Surfaces. *Adv. Funct. Mater.* **2010**, *20*, 3634−3645.

(2) Tong, H.; Ouyang, S. X.; Bi, Y. P.; Oshikiri, M.; Umezawa, N.; Oshikiri, M.; Ye, J. H. Nano-Photocatalytic Materials: Possibilities and Challenges. *Adv. Mater.* **2012**, *24*, 229−251.

(3) Zhou, K. B.; Li, Y. D. Catalysis Based on Nanocrystals with Well-Defined Facets. *Angew. Chem., Int. Ed.* **2012**, *51*, 602−613.

(4) Yang, H. G.; Liu, G.; Qiao, S. Z.; Sun, C. H.; Jin, Y. G.; Smith, S. C.; Zou, J.; Cheng, H. M.; Lu, G. Q. Solvothermal Synthesis and Photoreactivity of Anatase TiO_2 Nanosheets with Dominant {001} Facets. *J. Am. Chem. Soc.* **2009**, *131*, 4078−4083.

(5) Jiang, J.; Zhao, K.; Xiao, X. Y.; Zhang, L. Z. Synthesis and Facet-Dependent Photoreactivity of BiOCl Single-Crystalline Nanosheets. *J. Am. Chem. Soc.* **2012**, *134*, 4473−4476.

(6) Xi, G. C.; Ye, J. H. Synthesis of Bismuth Vanadate Nanoplates with Exposed {001} Facets and Enhanced Visible-Light Photocatalytic Properties. *Chem. Commun.* **2010**, *46*, 1893−1895.

(7) Liu, H.; Luo, M.; Hu, J. C.; Zhou, T. F.; Chen, R.; Li, J. L. β-Bi_2O_3 and Er^{3+} Doped β-Bi_2O_3 Single Crystalline Nnanosheets with Exposed Reactive {001} Facets and Enhanced Photocatalytic Performance. *Appl. Catal., B* **2013**, *140*, 141−150.

(8) Zhang, D. Q.; Wang, S. L.; Zhu, J.; Li, H. X.; Lu, Y. F. WO_3 Nanocrystals with Tunable Percentage of (001)-Facet Exposure. *Appl. Catal., B* **2012**, *123*, 398−404.

(9) Zhou, Y.; Tian, Z. P.; Zhao, Z. Y.; Liu, Q.; Kou, J. H.; Chen, X. Y.; Gao, J.; Yan, S. C.; Zou, Z. G. High-Yield Synthesis of Ultrathin and Uniform Bi_2WO_6 Square Nanoplates Benefitting from Photocatalytic Reduction of CO_2 into Renewable Hydrocarbon Fuel under Visible Light. *ACS Appl. Mater. Interfaces.* **2011**, *3*, 3594−3601.

(10) Jin, R.; Su, M. Y.; Wang, J.; Zhang, P.; Cui, M.; Chen, Y.; Yang, H. Q. Synthesis and Enhanced Photocatalytic Activity of Monodisperse Flowerlike Nanoarchitectures Assembled from CdS Nanoflakes with Exposed {001} Facets. *Mater. Res. Bull.* **2012**, *47*, 3070−3077.

(11) Bi, Y. P.; Ouyang, S. X.; Umezawa, N.; Cao, J. Y.; Ye, J. H. Facet Effect of Single-Crystalline Ag_3PO_4 Sub-Microcrystalson Photocatalytic Properties. *J. Am. Chem. Soc.* **2011**, *133*, 6490−6492.

(12) Zhao, H.; Yin, W. Y.; Zhao, M. Y.; Song, Y. Z.; Yang, H. Q. Hydrothermal Fabrication and Enhanced Photocatalytic Activity of Hexagram Shaped InOOH Nanostructures with Exposed {020} Facets. *Appl. Catal., B* **2013**, *130*, 178−186.

(13) Zheng, Z. K.; Huang, B. B.; Wang, Z. Y.; Guo, M.; Qin, X. Y.; Zhang, X. Y.; Wang, P.; Dai, Y. Crystal Faces of Cu_2O and Their Stabilities in Photocatalytic Reactions. *J. Phys. Chem. C* **2009**, *113*, 14448−14453.

(14) Sun, S. D.; Song, X. P.; Sun, Y. X.; Deng, D. C.; Yang, Z. M. The Crystal-Facet-Dependent Effect of Polyhedral Cu_2O Microcrystals on Photocatalytic Activity. *Catal. Sci. Technol.* **2012**, *2*, 925−930.

(15) Wöllenstein, J.; Burgmair, M.; Plescher, G.; Sulima, T.; Hildenbrand, J.; Böttner, H.; Eisele, I. Cobalt Oxide Based Gas Sensors on Silicon Substrate for Operation at Low Temperatures. *Sens. Actuators, B* **2003**, *93*, 442−448.

(16) Liao, L.; Zhang, Q. H.; Su, Z. H.; Zhao, Z. Z.; Wang, Y. N.; Li, Y.; Lu, X. X.; Wei, D. G.; Feng, G. Y.; Yu, Q. K.; Cai, X. J.; Zhao, J. M.; Ren, Z. F.; Fang, H.; Robles-Hernandez, F.; Baldelli, S.; Bao, J. M. Efficient Solar Water-Splitting Using a Nanocrystalline CoO Photocatalyst. *Nat. Nanotechnol.* **2014**, *9*, 69−73.

(17) Panagiotopoulos, I.; Alexandrakis, V.; Basina, G.; Pal, S.; Srikanth, H.; Niarchos, D.; Hadjipanayis, G.; Tzitzios, V. Synthesis and Magnetic Properties of Pure Cubic CoO Nanocrystals and Nanoaggregates. *Cryst. Growth Des.* **2009**, *9*, 3353−3358.

(18) Peng, C. X.; Chen, B. D.; Qin, Y.; Yang, S. H.; Li, C. Z.; Zuo, Y. H.; Liu, S. Y.; Yang, J. H. Facile Ultrasonic Synthesis of CoO Quantum Dot/Graphene Nanosheet Composites with High Lithium Storage Capacity. *ACS Nano* **2012**, *6*, 1074−1081.

(19) Zhang, M.; Wang, Y.; Jia, M. Q. Three-Dimensional Reduced Graphene Oxides Hydrogel Anchored with Ultrafine CoO Nanoparticles as Anode for Lithium Ion Batteries. *Electrochim. Acta* **2014**, *129*, 425−432.

(20) Koshizaki, N.; Yasumoto, K.; Sasaki, T. A Gas-Sensing CoO/SiO_2 Nanocomposite. *Nanostruct. Mater.* **1999**, *12*, 971−974.

(21) Ghosh, M.; Sampathkumaran, E. V.; Rao, C. N. R. Synthesis and Magnetic Properties of CoO Nanoparticles. *Chem. Mater.* **2005**, *17*, 2348−2352.

DOI: 10.1021/am508357x
ACS Appl. Mater. Interfaces 2015, 7, 6109−6117

(22) Li, L. P.; Sun, X. F.; Qiu, X. Q.; Xu, J. X.; Li, G. S. Nature of Catalytic Activities of CoO Nanocrystals in Thermal Decomposition of Ammonium Perchlorate. *Inorg. Chem.* **2008**, *47*, 8839−8846.
(23) Nam, K. M.; Shim, J. H.; Han, D. W.; Kwon, H. S.; Kang, Y. M.; Li, Y.; Song, H.; Seo, W. S.; Park, J. T. Syntheses and Characterization of Wurtzite CoO, Rocksalt CoO, and Spinel Co_3O_4 Nanocrystals: Their Interconversion and Tuning of Phase and Morphology. *Chem. Mater.* **2010**, *22*, 4446−4454.
(24) Sun, G. B.; Zhang, X. Q.; Cao, M. H.; Wei, B. Q.; Hu, C. W. Facile Synthesis, Characterization, and Microwave Absorbability of CoO Nanobelts and Submicrometer Spheres. *J. Phys. Chem. C* **2009**, *113*, 6948−6954.
(25) Yang, G. J.; Gao, D. Q.; Shi, Z. H.; Zhang, Z. H.; Zhang, J.; Zhang, J. L.; Xue, D. S. Room Temperature Ferromagnetism in Vacuum-Annealed CoO Nanospheres. *J. Phys. Chem. C* **2010**, *114*, 21989−21993.
(26) Yang, H. M.; Ouyang, J.; Tang, A. D. Single Step Synthesis of High-Purity CoO Nanocrystals. *J. Phys. Chem. B* **2007**, *111*, 8006−8013.
(27) Buck, M.; Biacchi, A.; Schaak, R. Insights into the Thermal Decomposition of Co(II) Oleate for the Shape-Controlled Synthesis of Wurtzite-Type CoO Nanocrystals. *Chem. Mater.* **2014**, *26*, 1492−1499.
(28) An, K.; Lee, N.; Park, J.; Kim, S. C.; Hwang, Y.; Park, J.; Han, M. J.; Yu, J.; Hyeon, T. Synthesis, Characterization, and Self-Assembly of Pencil-Shaped CoO Nanorods. *J. Am. Chem. Soc.* **2006**, *128*, 9753−9760.
(29) Jiang, J.; Liu, J. P.; Ding, R. M.; Ji, X. X.; Hu, Y. Y.; Li, X.; Hu, A. Z.; Wu, F.; Zhu, Z. H.; Huang, X. T. Direct Synthesis of CoO Porous Nanowire Arrays on Ti Substrate and Their Application as Lithium-Ion Battery Electrodes. *J. Phys. Chem. C* **2010**, *114*, 929−932.
(30) Zhang, Y. L.; Zhu, J.; Song, X.; Zhong, X. H. Controlling the Synthesis of CoO Nanocrystals with Various Morphologies. *J. Phys. Chem. C* **2008**, *112*, 5322−5327.
(31) Delley, B. An All-Electron Numerical Method for Solving the Local Density Functional for Polyatomic Molecules. *J. Chem. Phys.* **1990**, *92*, 508−517.
(32) Perdew, J. P.; Burke, K.; Ernzerhof, M. Generalized Gradient Approximation Made Simple. *Phys. Rev. Lett.* **1996**, *77*, 3865−3868.
(33) Hirshfeld, F. L. Bonded-Atom Fragments for Describing Molecular Charge Densities. *Theor. Chim. Acta.* **1997**, *44*, 129−138.
(34) Boettger, J. C. Nonconvergence of Surface Energies Obtained from Thin-Film Calculations. *Phys. Rev. B* **1994**, *49*, 16798−16800.
(35) Liu, B.; Wei, A. H.; Zhang, J. Y.; An, L. J.; Zhang, Q. Q.; Yang, H. Q. Synthesis and Photocatalytic Activity of Monodisperse Single Crystalline NiO Octahedrons by the Selective Adsorption of Cl^- Ions. *J. Alloy. Compd.* **2012**, *544*, 55−61.
(36) Wang, Z. L. Transmission Electron Microscopy of Shape-Controlled Nanocrystals and Their Assemblies. *J. Phys. Chem. B* **2000**, *104*, 1153−1175.
(37) Liang, Q.; Zhao, H.; Ning, L. C.; Wang, J. L.; Zhang, C. J.; Wang, L.; Wei, A. H.; Zhao, Q.; Yang, H. Q.; Liu, S. Z. InOCl Nanosheets with Exposed {001} Facets: Synthesis, Electronic Structure, and Surprisingly High Photocatalytic Activity. *Appl. Catal., B* **2013**, *152*, 390−396.
(38) Hoffmann, M. R.; Martin, S. T.; Choi, W.; Bahneman, D. W. Environmental Applications of Semiconductor Photocatalysis. *Chem. Rev.* **1995**, *95*, 69−96.
(39) Chen, C. C.; Ma, W. H.; Zhao, J. C. Semiconductor-Mediated Photodegradation of Pollutants Under Visible-Light Irradiation. *Chem. Soc. Rev.* **2010**, *39*, 4206−4219.
(40) Sobana, N.; Swaminathan, M. The Effect of Operational Parameters on the Photocatalytic Degradation of Acid Red 18 by ZnO. *Sep. Purif. Technol.* **2007**, *56*, 101−107.
(41) Zhang, Z. Y.; Shao, C. L.; Li, X. H.; Wang, C. H.; Zhang, M. Y.; Liu, Y. C. Electrospun Nanofibers of p-Type NiO/n-Type ZnO Heterojunctions with Enhanced Photocatalytic Activity. *ACS Appl. Mater. Interfaces.* **2010**, *2*, 2915−2923.
(42) Jiao, Y.; Liu, Y.; Yin, B. S.; Zhang, S. W.; Qu, F. Y.; Wu, X. Hybrid α-Fe_2O_3@NiO Heterostructures for Fiexible and High-Performance Supercapacitor Electrodes and Visible Light Driven Photocatalysts. *Nano Energy* **2014**, *10*, 90−98.
(43) Zong, X.; Yan, H. J.; Wu, G. P.; Ma, G. J.; Wen, F. Y.; Wang, L.; Li, C. Enhancement of Photocatalytic H_2 Evolution on CdS by Loading MoS_2 as Cocatalyst under Visible Light Irradiation. *J. Am. Chem. Soc.* **2008**, *130*, 7176−7177.

DOI: 10.1021/am508357x
ACS Appl. Mater. Interfaces 2015, 7, 6109−6117